Acta
Technica
Jaurinensis

Vol. 11, No. 3, pp. 119-131, 2018
DOI: 10.14513/actatechjaur.v11.n3.435
Available online at acta.sze.hu

Defining the Temperature Change of the Brake Disc

M. Menyhártné Baracskai

Széchenyi István University
Department of Mechatronics and Machine Design
H-9026 Győr, Hungary, Egyetem tér 1.
e-mail: baramel@sze.hu

Abstract: In the article the thermal analysis of the brake disc and separator disc of a high performance power machine will be presented. As example an agricultural vehicle with weight of 30000 kg and maximum travel speed of 40 km/h will be taken. At stopping the vehicle, the braking system located in the wheel body becomes activated. The traversing of the piston forces the brake discs to friction. Therefore significant amount of heat is generated, which needs to be derived from the system. The article presents the construction of the disc brake system. Providing boundary condition, the radial temperature change of the cooled part of the brake disc will be defined.

Keywords: agricultural vehicle, disc brake, brake oil, braking, temperature

1. Description of braking from the thermal aspect

As shown on Figure 1 the disc brake equipment is located in the wheel body. During motion of the vehicle, while there is no braking, the brake equipment is in open position. The individual discs are not in contact with each other. The brake house is filled with oil up to 19 mm height over the shaft centre. Heat exchanging processes are carried out between the elements of the equipment in contact with oil. During braking, the hydraulic presses the rotating discs, therefore they are closing. A featuring characteristic of the brake discs is that they are equipped with grooved friction surface. During braking, the cooling oil leaves the system through the grooves and heat exchanging processes are carried out between the discs in contact with each other. When braking is completed, the discs open up again and the oil re-

flows into the brake discs between. It warms up there and cause the centrifugal force as result of the rotating move, the oil is splashed against the wall of the brake house. Some of the generated amount of heat is passed on to the environment. The part of the heat remaining in the system is derived by a water cooling heat exchanger. The oil cooler connected to the subject unit is equipped with a pump providing 16 litres/min flow rate, through which the oil is delivered.

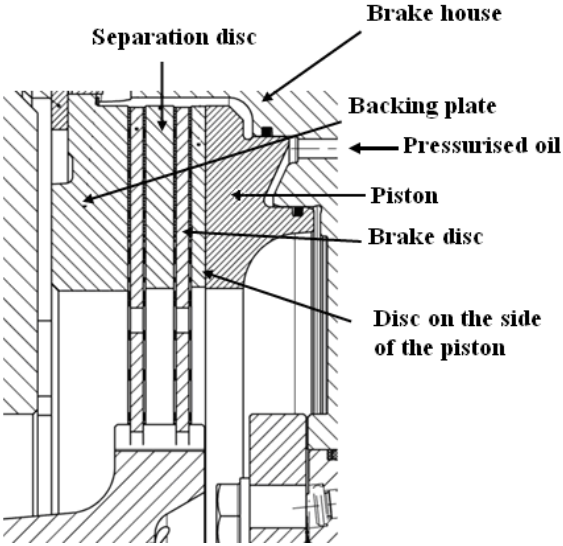

Figure 1. Major elements inside the wheel body

2. Description of the temperature values necessary for the calculations

By using temperature sensor located in the separator disc the generated temperature was measured. During the measurement braking was examined at a slowing rate of 2 m/s^2 from 40 km/h until completely stopping. As the result of the braking, the highest temperature of the brake disc 234°C is obtained. Prior to writing the differential equation, computer aided simulation was carried out on the brake unit for the purpose of learning the average temperature values generated on the biggest radius of each disc. For the simulation Nastran software was used. As result of the simulation the temperature on the external radius of the separator disc is 186.7°C, and in case of the brake disc is 172.2°C.

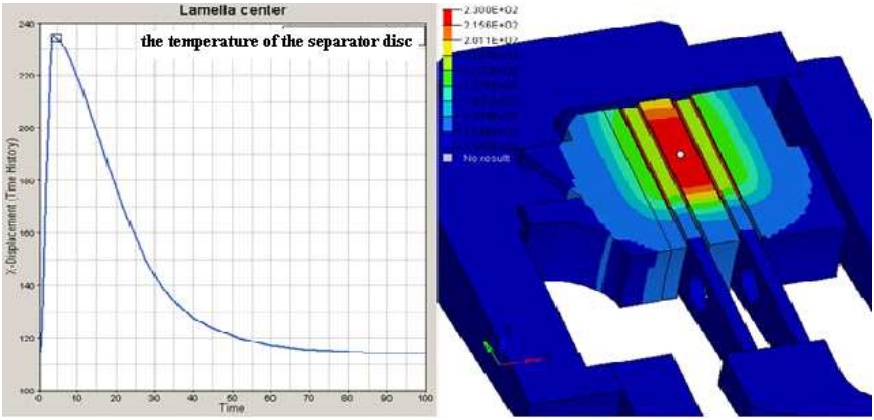

Figure 2. Results of the computer aided simulation

As on the diagram can be seen, during the braking the temperature in the place of the measuring device placed inside the separator disc increases to 234 °C, then, as a result of the heat derivation by the cooling oil, drops very quickly to 115 °C.

As shown on the Figure the separator disc receives the highest heat load. The asbestos friction layer pressed on the two sides of the brake discs have rather poor heat conduction capacity almost insulating the discs. That is why the temperature of the brake discs is lower, while the friction layer is high, reaches 230 °C.

3. Writing the heat conduction-exchange differential equation for the cooled part of the brake disc in order to define the temperature rate distribution of the disc.

During the braking process, the energy of motion of the vehicle turns to be work of friction, whereas heat is generated. As the result of braking, the upper part of the brake disc and of the separator disc are subject to bearing quite high heat load. The lower part of the discs is being cooled. The heat conduction-exchange differential equation for the cooled part of the brake disc can be formed.

The temperature change of the disc needs to be defined in order to see the life cycle in use and shelf life of the brake oil. The life cycle of the brake oil was analysed with Differential Scanning Calorimeter (DSC) in inert (nitrogen) atmosphere. The results of the oil analysis gained through the help of the DSC device are to be presented in Article [12].

The life cycle of the oil is definitely featured by the boundary layer of the oil adhering on the disc. The temperature of the boundary layer almost equals with that of the disc. Therefore the temperature change of the disc needs to be examined. [10]

The temperature change of the disc in balance of the radius has to be defined by a heat conduction-exchange differential equation written for one element of the rotating disc. It is presented in the following.

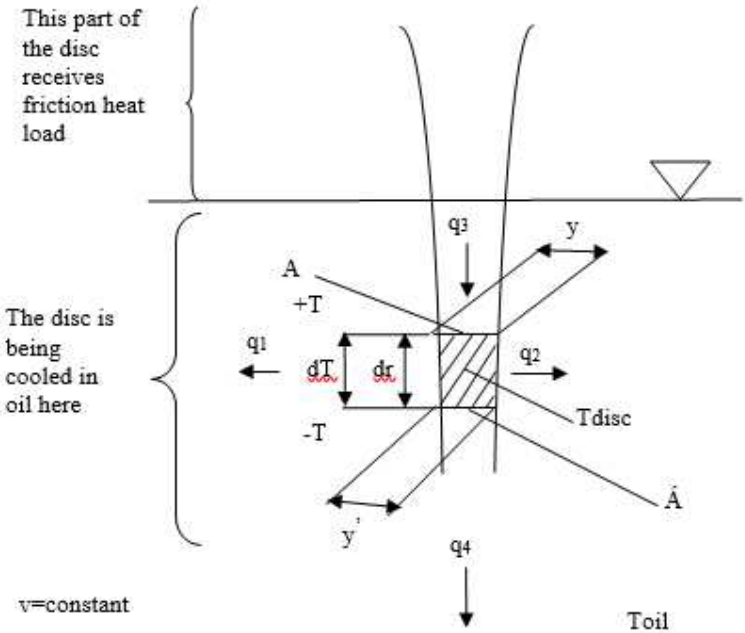

Figure 3. Dimensions of one element of the disc and the heat loads acting upon it

Whereas:

q1 and *q2* are the heat mounts leaving through the wall of the element by heat transfer (because of the oil cooling)

q3 and *q4* are the heat mounts leaving through the horizontal surface of the disc by heat conduction.

T is the temperature of the examined element

Toil is the temperature of the cooling oil

A is the surface of the disc element provided on the heat conduction side radius (*r*+*dr*) of the disc

Á is the surface provided on the r radius

As the result of braking, the temperature of the separator disc is increasing to the highest value of all the parts of the brake system. Therefore is reasonable to write the heat conduction-exchange differential equation for the separate disc. The temperature on the external radius of the separator disc, where cooling begins is 186.7 °C. The temperature of the cooling oil can be considered as constant to be 80 °C since a high flow rate pump immediately forwards the cooling heated oil to the water-cooled oil cooler.

As boundary condition, 186.7 °C temperature is taken in one point of the diameter of the separator disc. This is because the subject is to examine the state belonging to the maximum heat load.

The temperature in the subject case does not change in time; however, it depends on the place. Only an amount of heat can enter the thermodynamic system, which is enough for maintaining the 186.7 °C as measured on the edge of the disc. Since the temperature of the cooling oil is lower than the temperature of the edge of the disc, therefore it is expected during the examination that the temperature of the brake disc will decrease towards the centre.

At writing the temperature, the entering and leaving amounts of heat need to be of 0 values. Further, the entering amount of heat will be +, while the leaving heat amount will be -.

$$+q_3 - q_4 - (q_1 + q_2) = 0 \tag{1}$$

Since the thickness of the disc element is changing, the calculation is two differentially altering surfaces while writing the equation.

$$\acute{A} = 2 \cdot \pi \cdot r \cdot y' \tag{2}$$

$$A = 2 \cdot \pi \cdot r \cdot y \tag{3}$$

where:
A is the surface of the examined element provided on the heat conduction side ($r+dr$) radius,
$\acute{A}$ is the surface provided on the r radius.

$$q_3 = \lambda \cdot 2 \cdot \pi \cdot r \cdot y \frac{dT}{dr} \tag{4}$$

$$q_4 = \lambda \cdot 2 \cdot \pi \cdot r \cdot y' \frac{dT}{dr} \tag{5}$$

If y=constant, and dr is of elemental size.

$$q_3 - q_4 = \lambda \cdot A\frac{dT}{dr} - \lambda \cdot A'\frac{dT'}{dr} = \lambda \frac{d}{dr}\left(A\frac{dT}{dr}\right)dr \tag{6}$$

The $\acute{A}<A$, $A\frac{dT}{dr}$ and the $A'\frac{dT'}{dr}$ are differentially altering from each other; therefore the equation sourcing from the heat conduction is:

$$\lambda d\left(A\frac{dT}{dr}\right) = \lambda \frac{d}{dr}\left(A\frac{dT}{dr}\right)dr = q_3 - q_4 \tag{7}$$

The heat amount leaving through the side walls of the element sources from the heat transfer between the disc and the oil. Since q1 and q2 are equal, a duplicator enters the equation.

$$q_1 + q_2 = 4 \cdot \alpha_{ol} \cdot \pi \cdot rdr\left(T_{disc} - T_{oil}\right) \tag{8}$$

where:
the α_{ol} is the oil heat transfer factor is constant along the radius of the disc.

The complete differential equation is given from the evaluation of the above tags with the right algebraical sign back to the heat balance:

$$\lambda \frac{d}{dr} \cdot \left(A_{(r)} \frac{dT_{(r)}}{dr}\right)dr - 4\alpha_{ol} \cdot \pi \cdot rdr\left(T_{disc} - T_{oil}\right) = 0 \tag{9}$$

With the exception of the heat conduction factor, all factors depend on the radius and the heat transfer factor of the oil is constant.

The direct solution of the (9) differential equation is rather complicated and long lasting. Even with providing certain conditions (disc and temperature rates etc.), it is only approximately possible. Therefore, the transformation of the equation to be a differential equation is taken by the choice. Although in principle it is less accurate, in case an appropriately low value Δr-s are selected, the final result would be eventually more accurate for it is not bond to various restricting conditions.

The second term in the equation can also be calculated directly as a differential equation, since (dr~ Δr), Tdisc(r) changes by ΔT.

Transferring the first term to be a differential equation is as follows.

The first term's $\left(A_{(r)} \frac{dT_{(r)}}{dr} \right)$-t as product is derived.

$$\lambda \left\{ \left[\frac{dA_{(r)}}{dr} \cdot \frac{dT_{(r)}}{dr} + A_{(r)} \frac{d^2 T_{(r)}}{dr^2} \right] \right\} dr \tag{10}$$

Let us divide the *r* radius (the cooled part) into *Δr* constants. $\sum \Delta r = r2 - r1$, where *r2*=150 mm is the initial radius of the part of the disc cooled with oil and *r1*=120 mm is the inner radius of the disc. At writing the differential equation, thickness *v*=constant.

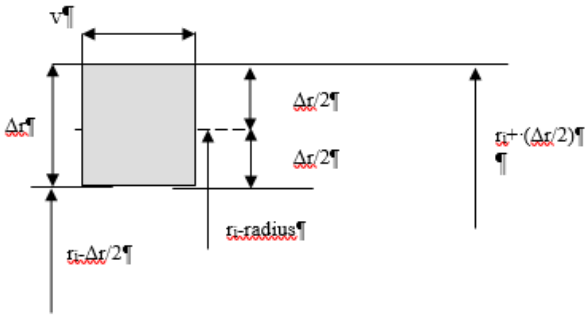

Figure 4. Writing of the differential equations

The differential equation taken in the r_i place

$$\frac{dA}{dr}\Big|_{r_i} \cong \frac{A_{\left(r_i + \frac{\Delta r}{2}\right)} - A_{\left(r_i - \frac{\Delta r}{2}\right)}}{\Delta r} \tag{11}$$

$$\frac{dT}{dr}\Big|_{r_i} \cong \frac{T_{\left(r_i + \frac{\Delta r_i}{2}\right)} - T_{\left(r_i - \frac{\Delta r_i}{2}\right)}}{\Delta r} \tag{12}$$

The $\frac{dA}{dr}\Big|_{r_i}$ value known from the distribution of the disc.

Transformation of the secondary differential:

$$\frac{d^2T}{dr^2} \approx \frac{1}{\Delta r}\left[\frac{T_{(r_i+\Delta r)} - T_{(r_i)}}{\Delta r} - \frac{T_{(r_i)} - T_{(r_i-\Delta r)}}{\Delta r}\right] = \frac{1}{\Delta r^2}\left[T_{(r_i+\Delta r)} - 2T_{(r_i)} + T_{(r_i-\Delta r)}\right] \quad (13)$$

Here, the difference of the two differential values was taken, since it is secondary. Since Δr occurs twice, Δri/2 shall be replaced by Δri-t. As per equation (13), the transferred secondary derived term still needs to be multiplied by the A(r) value.

$$A_{(r)}\frac{d^2T}{dr^2} = A_{(ri)}\frac{1}{\Delta r^2}\left[T_{(r_i+\Delta r)} - 2T_{(r_i)} + T_{(r_i-\Delta r)}\right] \quad (14)$$

The term $\left[T_{(r_i+\Delta r)} - 2T_{(r_i)} + T_{(r_i-\Delta r)}\right]$ is little; its value is practically zero.

The complete differential equation is formed as follows:

$$\lambda\left\{\begin{array}{l}\left[\dfrac{A_{\left(r_i+\frac{\Delta r}{2}\right)} - A_{\left(r_i-\frac{\Delta r}{2}\right)}}{\Delta r}\right]\left[T_{\left(r_i+\frac{\Delta r}{2}\right)} - T_{\left(r_i-\frac{\Delta r}{2}\right)}\right] + \\ + A_{(ri)}\dfrac{1}{\Delta r^2}\left[T_{(r_i+\Delta r)} - 2T_{(r_i)} + T_{(r_i-\Delta r)}\right]\end{array}\right\} - 4\alpha_{olaj}\pi r_i \Delta r\left(T_{disc} - T_{oil}\right) = 0 \quad (15)$$

The ΔT(r) value can be expressed from the differential equation with the following solutions:

- the geometrical values are known,
- λ; αoil; Toil; values are known,
- the values of the first term [ ] can be explicitly calculated,
- the second term [ ] this the Δri –size disc element, the ΔTi is the temperature change,
- the value of the third term is with a fair estimation is zero.

All elements are known in the fourth element, with the exception of Ti. The Ti is the average temperature of the ith disc element.

$$T_i = T_{\left(i+\frac{\Delta r}{2}\right)} - \Delta T_{(i)} \quad (16)$$

Therefore, the only remaining unknown element of the differential equation is ΔTi. With that, the next disc element becomes calculable up to the inner disc diameter. Therefore, the disc temperature change can be defined, which, with a fair estimation

is the same as the temperature in the boundary layer of the cooling oil. This temperature defines the life cycle of the oil.

4. The heat distribution of the separator disc

The following data were used at solving the equation:

- the largest radius of the separator disc is r_{et1}=224.8 mm,
- the smallest radius of the separator disc is r_{et2}=148.5 mm,
- the temperature of the cooling oil T_{oil}=80°C,
- the temperature of the largest radius of the separator disc to be cooled T_{et}=186.7 °C,
- thickness of the subject disc v_{et}=12 mm,
- the heat transfer factor of the cooling oil α_{oil}=1300 W/m^{2}K [11],
- the heat conduction factor relevant to the disc λ_{et}=50 W/mK [11],
- the calculation frequency taken at defining the radial temperature change of the disc: ΔR=0.1 mm.

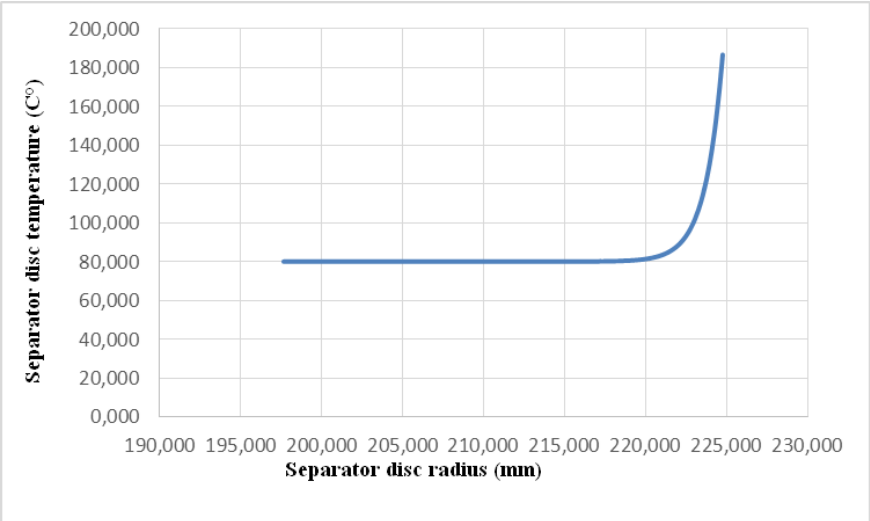

Figure 5. Radial heat change of the separator disc

The temperature of the separator disc, according to the boundary condition decreases towards the centre of the disc. Since only an amount of heat enters the system that is enough for maintaining the temperature on the largest radius of the disc, the temperature becomes equalized after a relatively few steps of calculation.

On the radius of 218.5 mm, the temperature will, with a fair estimation, be approximately the same as that of the cooling oil.

Similarly to the separator disc, the lower part of the brake disc is also set in cooling oil along the braking process, at which the upper part of the brake disc, similarly to the separator disc receives significant heat load. The heat exchange differential equation can also be written on this part of the disc being cooled in oil.

5. The heat distribution of the brake disc

The following data were used at solving the equation:

- largest radius of the brake disc r_{ft1}=224.4 mm,
- smallest radius of the brake disc r_{ft2}= 150 mm,
- temperature of the cooling oil T_{oil}=80°C,
- temperature of the largest radius of the brake disc to be cooled T_{ft}=172.2°C,
- thickness of the subject disc v_{ft}=5 mm,
- heat exchange factor of the subject disc α_{oil}=1300 W/m^{2}K [11],
- heat exchange factor relevant to the subject disc λ_{ft} =43 W/mK [11],
- at defining the radial temperature change of the disc, the calculation frequency taken is ΔR=0.1mm.

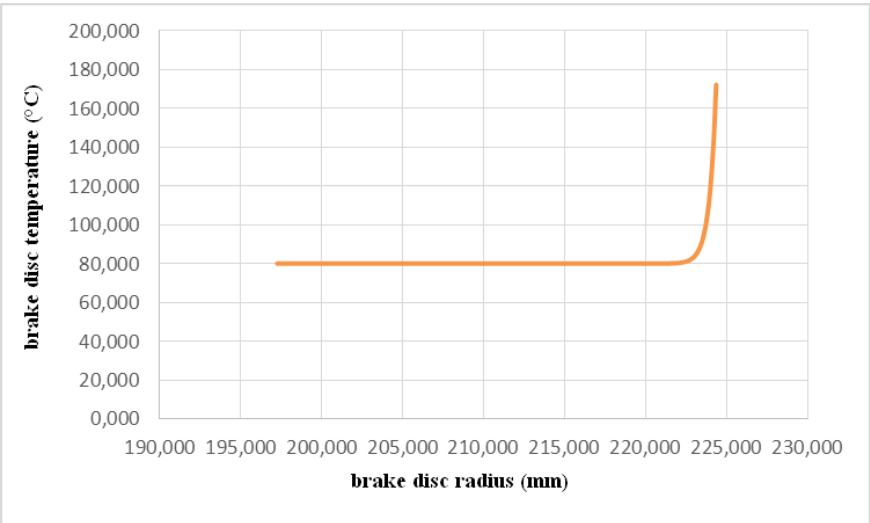

Figure 6. Radial heat change of the brake disc

As shown on the Figure 6, the result curve is similar to the result curve of the separator disc, it is because during writing the problem, same boundary conditions were used. Difference between the result curves can not only be seen because of the initial temperature but also due to the disc thickness and the significant difference of the heat changing factor as well. The disc already drops its temperature to that of the cooling oil already on the radius of 222 mm.

As can be seen from the results, the temperature of the disc drops in balance with the decrease of the radius concerned. Its maximum temperature is at the external radius (where the calculation begins), where this is the boundary condition.

The oil does not start being spoiled even at the maximum temperature of the disc material. The oil does not get damaged at the smaller radius of the disc since the temperature of the oil adhering to the boundary layer is smaller all around than the damaging temperature of the oil.

6. Summary

Following the short description of the brake unit, the study defines boundary conditions and writes a differential equation, with the help of which the temperature distribution of the part of the disc set in oil can be defined. After transferring the differential equation to derivation, the equation becalms possible to be solved even numerically. The author presents the radial heat distribution of the separator disc.

Acknowledgement

Special thank to Dr. Zobory István prof. emeritus who helped me in transforming the differential equation into differential equation, and to Takács Krisztián for the simulation results.

References

[1] W. I. Lokaj, M. N. Bodunow, W. I. Dewjatow, Kühlung bestimmte Elementen GTU, hergestellt AN. Sowjetunion/UDSSR, OTN, Energie und Transport, (3) (1968)

[2] M. Menyhártné Baracskai, Power Engineering of Brake System of a Heavy Duty Agricultural Motor Vehicle, Acta Mechanica Slovaca, 18 (2) (2014) pp. 28-35.

[3] J. S. Jiang, Analysis on Wet Multi-Disc Brake Based on ABAQUS, Advanced Materials Research, 421 (2012) pp. 427-430.
DOI: 10.4028/www.scientific.net/AMR.421.427

[4] C. Spulber, S. Voloaca, Comparison between some Simulation Methods Regarding the Thermal Stress on Disc Brake, Applied Mechanics and Materials, 325-326 (2013) pp. 135-141.
DOI: 10.4028/www.scientific.net/AMM.325-326.135

[5] J. Zhang, C. G. Xia, Research of the Transient Temperature Field and Friction Properties on Disc Brakes, Advanced Materials Research, 756-759 (2013) pp. 4331-4335.
DOI: 10.2991/iccia.2012.49

[6] M. Bogdevicius, J. Janutėnienė, O. Vladimirov, Simulation of Hydrodynamics Processes of Hydraulic Braking System of Vehicle, Solid State Phenomena, 147-149 (2009) pp. 296-301.
DOI: 10.4028/www.scientific.net/SSP.147-149.296

[7] J. B. Wang, M. Han, D. Y. Yu, Appropriate Mass Flow Research of Lubricant for Different Oil Groove Type of Wet Multi-Disc, Advanced Materials Research, 490-495 (2012) pp. 2366-2370.
DOI: 10.4028/www.scientific.net/AMR.490-495.2366

[8] X. J. Zheng, T. H. Luo, C. Jia, Dynamic Response Modeling of Fluid-Solid Coupling for Wet Brake Disc, Applied Mechanics and Materials, 475-476 (2014) pp. 1397-1401.
DOI: 10.4028/www.scientific.net/AMM.475-476.1397

[9] Z. Hu, M. Han, Z. C. Song, K. Y. Ning, Numerical Investigation on Thermo Mechanical Behavior in Wet Multidisc Friction Pairs System, Applied Mechanics and Materials, 697 (2015) pp. 177-180.
DOI: 10.4028/www.scientific.net/AMM.697.177

[10] E. Pásztor, Untersuchung der Wirkung der Kühlung von Gasturbinen – Scheiben, Periodica Politechnica. Ser. Transp. Eng., 34 (1-2) (2006) pp.85-92.

[11] K. Ražnjević, Thermal Technical Tables, Műszaki Könyvkiadó, Budapest, 1964, in Hungarian.

[12] W. Zielenkiewicz, E. Margas, Theory of Calorimetry, Kluwer Academic Publishers, Dordrecht, 2002.

[13] Z. Hu, M. Han, Z. C. Song, K. Y. Ning, Numerical Investigation on Thermo Mechanical Behavior in Wet Multidisc Friction Pairs System, Applied Mechanics and Materials, 657 (2015) pp. 177-180.
DOI: 10.4028/www.scientific.net/AMM.697.177

[14] F. Talati, S. Jalalifar, Analysis of heat conduction in a disk brake system, Heat and mass transfer, 45 (8) (2009) pp. 1047-1059.
DOI: 10.1007/s00231-009-0476-y

[15] H. Mazidi, S. Jalalifar, J. Chakhoo, Mathematical modeling of heat conduction in a disk brake system during braking, Asian Journal of Applied Sciences, 4 (2) (2011) pp. 119-136.
DOI: 10.3923/ajaps.2011.119.136

[16] O. Huajiang, N. Wayne, Y. Yuan, F. Chen, Numerical analysis of automotive disc brake squeal: A review, International Journal of Vehicle Noise and Vibration, 1 (3-4) (2005) pp. 207-230.
DOI: 10.1504/IJVNV.2005.007524

[17] M. Menyhártné Baracskai, K. Takács, Thermal analysis and optimization of oily disc brakes of a high performance vehicle, Hadmérnök 12 (2) (2017) pp. 299-309, in Hungarian

Acta
Technica
Jaurinensis

Vol. 11, No. 3, pp. 132-149, 2018
DOI: 10.14513/actatechjaur.v11.n3.457
Available online at acta.sze.hu

Parallel Numerical Creation of Phase-space Diagrams of Nonlinear Systems Using Maple

F. Hajdu, Gy. Molnárka

Széchenyi István University, Faculty of Mechanical Engineering, Informatics and Electrical Engineering, Department of Mechatronics and Machine Design
Egyetem tér 1., 9026 Győr, Hungary
e-mail: hajdfl@sze.hu

Abstract: In this paper the numerical creation of phase-plane diagrams in parallel utilizing Maple is presented. One of the most effective method for studying nonlinear systems is the creation of detailed enough phase-plane diagrams. But in the case of large systems it requires huge amount of numerical calculation, which can be accelerated using parallel computers. Here we show some attempts for this using moderate size known problems. We demonstrate that detailed diagrams can be created fast and efficiently with a SIMD model based algorithm even using simple PC-s. We exhibit that the parallel algorithm taken for one- and two-dimensional problems can be expanded for 3D phase-space diagram creation without any loss of efficiency. In this paper a methodology is showed which can be followed in the study of large dynamical systems as well.

Keywords: parallel computing, SIMD, Maple, numerical analysis, nonlinear system modeling

1. Introduction

One effective way for the study of nonlinear differential system of equations is the construction of the detailed enough phase space diagrams 145. For construction of such diagrams we can construct numerical algorithms with many arithmetic operations. However these algorithms are easily parallelizable, so the map of phase space can be drawn with high resolution and very fast using many processors or supercomputers. In our research work we begin with the program of Parallel Maple because it provides algorithms for solving differential equations and two models for

parallelization. The paper first introduces the parallelization possibilities with Maple. In the next part in our paper we briefly describe the sequential and parallel algorithms to create the phase-plane diagram. In the next section the tests and results with the parallel program are described in detail. The paper concludes with further development tasks and the summary of the achieved results.

2. Parallelization with Maple

Maple provides two models for parallelization: the thread-based Task programming model, which enables parallelization by executing multiple tasks within a single process and the Grid programming model with starting multiple processes [2]. The main difference between the two models is the memory access: former uses a shared memory (SMP), latter a distributed memory (DMP) [3].

In [4] both of them was tested and compared. As the problem size increased the Grid programming model operated increasingly better, with surprisingly good results at the highest resolution. For solving larger problems the Task programming model seemed less suitable. Not only memory sharing problems occurred, but the speedup and the efficiency also decreased with increasing resolution. Grid programming model was chosen for further research.

Parallelized Maple has already been used for solving arithmetic problems [5], parallel symbolic computation [6], [7], [8], operations with polynomials[9], [10], solving initial value problems for ordinary differential equations [11],[12] and solving nonlinear algebraic problems [13], [14], .

The development of using Maple in parallel started in the 1990s, there were a lot of approach. First there were interfaces between Maple and another programming environment (C/Linda [5], Strand[6], C++[8], Eden[13]) capable of parallelization. There are examples of extended Maple kernels [9] and grid enabling wrappers [16] too. Distributed Maple was an approach of using Maple parallel without any external interface [14]. Nowadays Maple's Grid Computing Toolbox is used for example for parallel operations with polynomials [17]. Parallelized Maple has been used on massively parallel, distributed memory machine [9] and computer clusters too [16].

The detailed description of parallelized Maple applications can be found in [4]. It can be seen that Maple was used mostly on distributed systems, which also confirms our results, that Maple Grid Programming model suits better for our task

3. Numerical creation of a state-space diagrams

3.1. Sequential algorithm

To construct the phase-plane diagrams the system of equation with many initial states was solved numerically. The initial states were stored in a list. For construction of a phase-plane diagram a sequential algorithm was used, which went through all the elements of a list. For numerical solution Maple's *dsolve* command was used with *rkf45* numerical solver [18].

In this study the sequential algorithm was expanded in a way to create 3D state-space diagrams. The sequential algorithm to construct the 3D state-plane diagram in case of *h* system variables and *h* differential equations can be seen in Figure 1.

The initial data for calculation should be specified. They are the initial states, the system parameters, and the system of equations. For defining the initial states sets were given for x1(0)-x2(0)-..-xh(0). Inside the sets x1(0)-x2(0)-..-xh(0) pairs are created, which are stored in a list. With changing the resolution inside sets the number of initial states could be varied.

The next step is solving the system of equations. Maple stores the solution in a procedure (*procrkf45*) [18]. This procedure can calculate the result at a given time. For constructing the phase-plane diagram a sequence is necessary for calculate the results at a given time period (*seq* command). Maple can store the results in a plot. All plots are collected in a list, which can be easily displayed after calculating the results for all of the initial states.

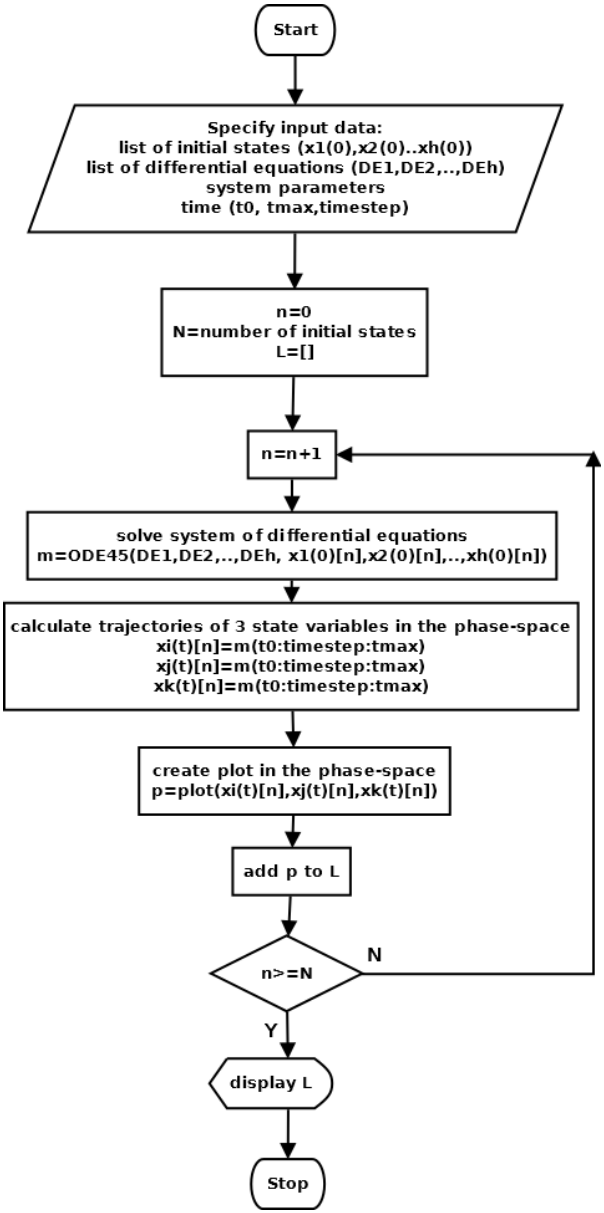

Figure 1. The flow chart of the sequential algorithm

3.2. Parallel algorithm

Constructing phase-plane diagrams in a numerical way can be easily parallelized. There are a lot of different input data (initial states), but the same calculations should be carried out with them. The parallelization therefore can be done according to SIMD model [19].

For parallelization using Maple's Grid Programming model a master node must be created to supervise slave nodes and arrange the data of the results. The slave nodes calculate the results for different initial states and send them to the master node. The flow chart for this model in Maple can be seen in Figure 2. The algorithm was based on [20].

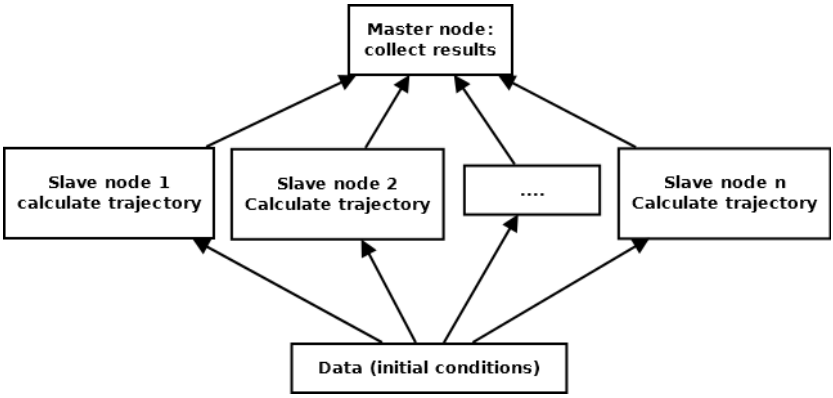

Figure 2. Flow chart of the parallel algorithm

4. Tests

The tests were carried out on a PC with an IntelCorei5-4460 @ 3200 Mhz CPU processor and 16 GB RAM. The processor has 4 cores. The equations for calculating the speedup (S) [21] and the relative speedup [22] (R) are:

$$S = \frac{T_s}{T_n} \tag{1}$$

$$R = \frac{S}{n} \tag{2}$$

where T_s is the sequential running time, T_n is the parallel running time and n is the number of cores.

This parallel algorithm was previously tested with the numerical creation of phase-plane diagrams of a Tunnel diode circuit [23]. The results were very promising, a 3 fold speedup could be achieved with a simple PC. In this study the phase-plane diagram of other 2 simple nonlinear systems were created: the Van der Pol oscillator and a biochemical reaction.

Van der Pol oscillator

The Van der Pol oscillator is a simple nonlinear oscillator [1]. From the phase-plane diagram of nonlinear oscillators also a lot of information can be derived, one of the most important one is the limit cycle (can be seen in Figure 1). The differential equation of the system is:

$$\frac{d^2}{dt^2}x(t) = \mu(1 - x(t)^2)\frac{d}{dt}x(t) - x(t) \tag{3}$$

For defining the initial states sets were given for x(0) and dx(0). The sets are [-3; 3] in both cases. This set was chosen in a way that the limit cycle is inside the set.

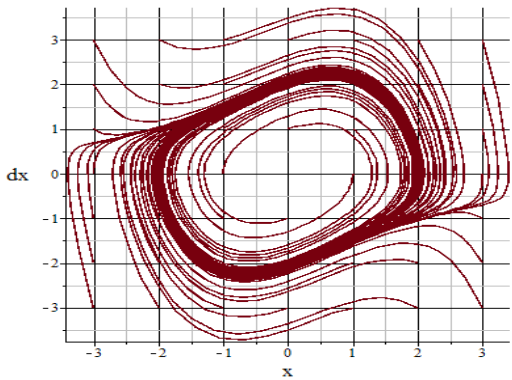

Figure 1. The phase-plane diagram of the Van der Pol oscillator (μ=1)

The results can be seen in Table 1 and in Figure 2.

Table 1. Average calculation times (T), speedup (S) and relative speedup (R) for constructing the phase-plane diagram of the Van der Pol oscillator

Resolution (number of initial states)		Sequential	Parallel (2 cores)	Parallel (4 cores)
0.5 (16)	T	3.439	2.869	1.255
	S		1.199	2.742
	R		0.599	0.685
1 (49)	T	10.686	7.737	3.479
	S		1.381	3.072
	R		0.691	0.768
2 (169)	T	37.19	26.768	11.451
	S		1.389	3.248
	R		0.695	0.812
4 (625)	T	146.422	98.358	42.541
	S		1.489	3.442
	R		0.744	0.860
8 (2401)	T	609.757	384.479	165.828
	S		1.586	3.677
	R		0.793	0.919

In Table 2 it can be seen that around a 3 fold speedup could be achieved with a 0.8 relative speedup in case of 4 cores. As the resolution increased the speedup and the efficiency increased, at the highest resolution over 90% efficiency could be achieved with almost a 4 fold speedup. In case of 2 cores a maximum 1.5 speedup could be achieved with a 0.8 relative speedup. Except the lowest resolution the efficiency was above 60% in all cases. The overhead is less using 4 cores in all cases. Better results could be achieved using 4 cores, therefore the algorithm is scalable. At higher resolution the increase in efficiency was better (>10%) using 4 cores, which means that larger problems are better scalable.

Further tests will be necessary in the future using supercomputers with more cores to examine the scalability of the algorithm in more detail.

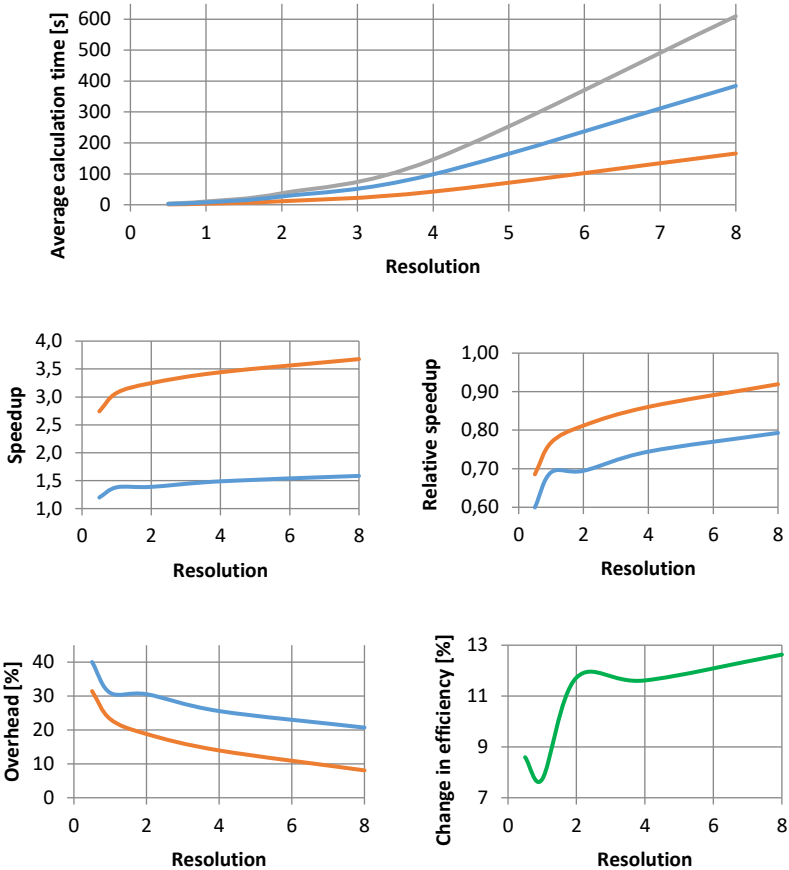

Figure 2. The average calculation time (up, grey: sequential, blue: 2 cores red: 4 cores), speedup (middle left), relative speedup (middle right), overhead (bottom left) and change in efficiency comparing 2 and 4 cores (bottom right) versus the resolution in case of creating the phase-plane diagram of the Van der Pol oscillator

First the increase is faster using both 2 and 4 cores, but after resolution 1 the increase slows down. Next task is to examine the changing in limit cycle as parameter μ is varied in parallel.

Creation of 3D state-space diagram: a biochemical reaction

The described algorithm was expanded for 3D tasks too, which means the creation of the state-space diagram. It was tested with a simple example with 3 variables. It is the model of a biochemical reaction [24]. The differential equation is:

$$\frac{dx(t)}{dt} = \frac{1}{\alpha}(x(t) + y(t) - x(t) \cdot y(t) - qx(t)^2) \tag{4}$$

$$\frac{dy(t)}{dt} = 2mz(t) - y(t) - x(t) \cdot y(t) \tag{5}$$

$$\frac{dz(t)}{dt} = \frac{1}{r}(x(t) - z(t) \tag{6}$$

where x(t), y(t) and z(t) are the species concentrations, α, q, m, r are constants. The state-space diagram can be seen in Figure 3. From the state-space diagram it can be seen that a limit cycle exists if α=0.1, q=0.01 , m=0.5 and r=1.

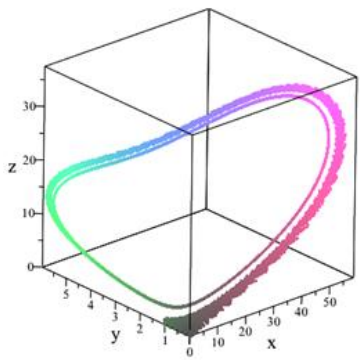

Figure 3. The phase-space diagram of a biochemical reaction

For defining the initial states sets were given for x(0), y(0) and z(0). The sets are [0; 1] for all variables.

The results can be seen in Table 2 and in Figure 4.

Table 2. Average calculation times (T), speedup (S) and relative speedup (R) for constructing the phase-space diagram of a biochemical reaction

Resolution (number of initial states)		Sequential	Parallel (2 cores)	Parallel (4 cores)
0.25 (27)	T	1.353	1.295	0.537
	S		1.045	2.521
	R		0.523	0.630
0.5 (216)	T	10.952	7.347	3.853
	S		1.491	2.842
	R		0.745	0.711
1 (1331)	T	63.478	45.068	18.735
	S		1.408	3.388
	R		0.704	0.847
2 (9261)	T	482.317	-	131.361
	S		-	3.672
	R		-	0.918

It can be seen that around 3 fold speedup could be achieved with 75% efficiency in case of 4 cores. For small resolutions the speedup was less than 3 and the efficiency less than 70%. After resolution 1 an over 3 fold speedup could be achieved with an above 80% efficiency. For the highest resolution a surprisingly good result could be achieved: 3.6 fold speedup with 92% efficiency. In case of 2 cores a maximum 1.5 fold speedup could be achieved with 75% efficiency at resolution 0.5. When the resolution was further increased both of them decreased. At the highest resolution the calculation failed because of lack of memory. The overhead was less using 2 cores at resolution 0.5, which means the algorithm is better scalable at higher

resolution. At resolution 1 a 14% increase in efficiency could be achieved using 4 cores.

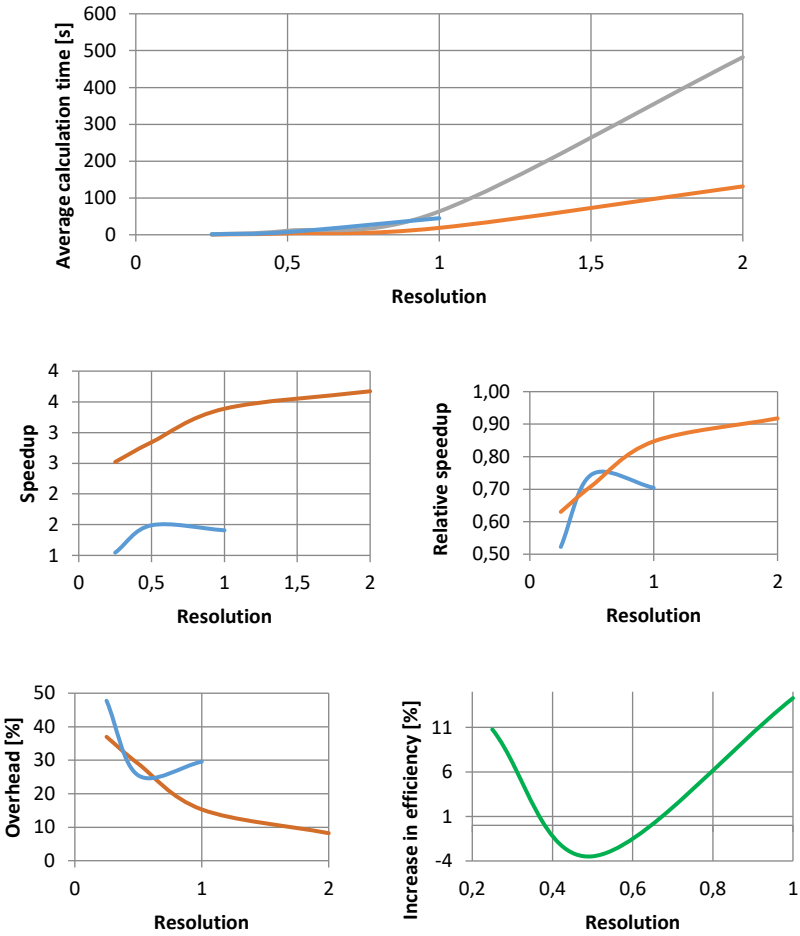

Figure 4. The average calculation time (up, grey: sequential, blue: 2 cores red: 4 cores), speedup (middle left), relative speedup (middle right), overhead (bottom left) and change in efficiency comparing 2 and 4 cores (bottom right) versus the resolution in case of creating the phase-space diagram of a biochemical reaction

The speedup and the efficiency up to resolution 1 is linear using 4 cores. After that is still remains linear, but the slope is smaller. With this test it was verified that this

algorithm is suitable also for creating 3D state-space diagrams in parallel very efficiently. The scalability of the algorithm should be examined with more cores in the future.

5. Further development

In this section the further development tasks are described. These are the possibilities of using supercomputers in the future and examining other more complex nonlinear systems with creation of phase-plane and other diagrams in parallel.

Using supercomputers

Our forthcoming research is to measure the speedup effect and examine the scalability of the algorithm on a supercomputer using a much more number of processors [25]. Three possibilities were examined

- using Maple
- connecting Maple to another environment
- use a completely different programming language

As we have limited number of Maple licenses it was discarded to use it on supercomputers.

Another possibility is to connect Maple to other parallel programming language. In the literature there are several examples, like Sugarbrush (Maple+C/Linda) [5],‖MAPLE‖ (Maple+Strand)[6], FoxBox (Maple + C++) [8], PVMaple (Maple + PVM) [11], Maple+Eden [13], OpenMaple+MPI [17]. Most of these solutions did not spread due their special kernel [14] or were not effective enough as format conversion can be very time consuming [13],[17].

The third possibility was chosen, which is to develop a parallel target program in C++. A demo program was already developed for creating the phase-plane diagram of a Tunnel diode circuit in parallel using OpenMp directives. Compared to parallel Maple another 6 fold speedup could be achieved on the same computer. More about the development of the demo program can be read in [26].

Other tasks

Further development task is to speedup the examination of other nonlinear systems as well and to create further high-performance computing workload diagrams like bifurcation diagrams [27] (seen in Figure 5) in parallel. For simple bistable systems, like the Tunnel diode circuit Maple command *implicitplot* is applicable. For fast creation of bifurcation diagrams of oscillators and more complex systems an iterative program based on [28] can be used. The parallelization of 3D bifurcation diagrams using the simple iterative algorithm has already been achieved [29].

Other future task is to create Poincaré sections [28] and frequency spectrum maps [30] also in parallel to facilitate the numerical examination of more complex nonlinear systems as well.

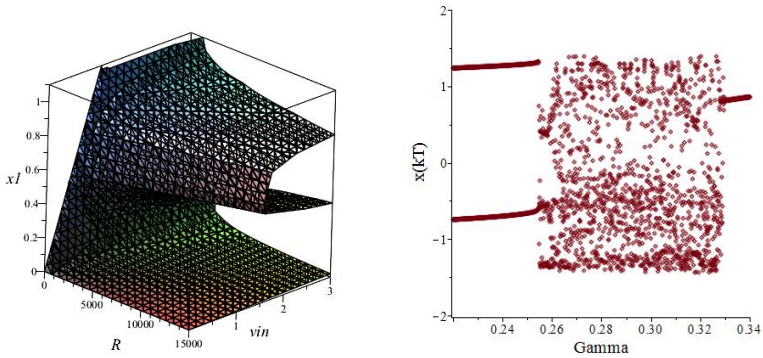

Figure 5. The 2 parametric bifurcation diagram of the Tunnel diode circuit (left)[23] and the bifurcation diagram of the Duffing-Holmes oscillator (right)

6. Conclusion

The numerical creation of the phase-plane diagrams of simple nonlinear systems in parallel was achieved with a SIMD model based algorithm utilizing Maple's Grid programming model. On a 4 core desktop an average 3 fold speedup could be achieved with an average 75-80% efficiency in all test cases. As the problem size

increased the parallel program operated increasingly better, with surprisingly good results at the highest resolutions. For simple nonlinear systems a detailed phase-plane and 3D phase space diagrams can be created fast and efficiently even on simple PC-s with limited number of cores. The presented method can be used for numerical examination of more complex dynamical systems in the future.

Acknowledgement

The publishing of this paper was supported by EFOP-3.6.1-16-2016-00017 project.

References

[1] H.K. Khalil, Nonlinear Systems, Prentice Hall, (1999)

[2] Maple help, 2016, [cited 01.10.2016] https://www.maplesoft.com/support/help/Maple/view.aspx?path=ProgrammingGuide/Chapter15

[3] S. Jin, S.E. Oh, J.W. Hong, Performance Evaluation of a Finite Element Code Parallelized with OpenMP, in P. Iványi, B.H.V. Topping, G. Várady, (Eds), Proceedings of the Fifth International Conference on Parallel, Distributed, Grid and Cloud Computing for Engineering, Civil-Comp Press, Stirlingshire, UK, Paper 36, (2017). DOI:10.4203/ccp.111.36

[4] F. Hajdu, Gy. Molnárka, Parallelization of Numerical Examination of Nonlinear Systems using Maple, in P. Iványi, B.H.V. Topping, G. Várady, (Eds), Proceedings of the Fifth International Conference on Parallel, Distributed, Grid and Cloud Computing for Engineering, Civil-Comp Press, Stirlingshire, UK, Paper 30, (2017). DOI:10.4203/ccp.111.30

[5] B. Char, J. Johnson, Some experiments with Parallel Bignum Aritmetic, in H. Hong (Ed) PASCO'94 Proceedings of First International Symposiumon Parallel Symbolic Computation, World Scientific Publishing Co., Inc. River Edge, NJ, USA, (1994)

[6] K. Siegl, Parallelizing Algorithms for Symbolic Computation using ‖MA PLE‖, in Proceedings of the fourth ACM SIGPLAN symposium on Principles

and practice of parallel programming, ACM New York, NY, USA, (1993), pp. 179–186.
DOI: 10.1145/155332.155351

[7] K.C. Chan, A. Diaz, E. Kaltofeln, A Distributed Approach to Problem Solving in Maple, in R.J. Lopez (Ed) Maple V: Mathematics and its Applications, Birkhäuser, Boston, (1994), pp. 13-21.

[8] A. Diaz, E. Kaltofeln, FOXBOX: A System for Manipulating Symbolic Objects in Black Box Representation, in "Proceedings of the 1998 international symposium on Symbolic and algebraic computation, ACM New York, NY, USA,(1998), pp. 30-37.

[9] L. Bernardin, Maple on a massively parallel, distributed memory machine, in M. Hitz (Ed) PASCO '97 Proceedings of the second international symposium on Parallel symbolic computation, ACM New York, NY, USA, (1997), pp. 217-222.
DOI: 10.1145/266670.266732

[10] J. Liu, S. Wu, H. Li, X. Yao, F. Du, Parallelization of Characteristic Series, in W. Wang (Ed) Mechatronics and Automatic Control Systems: Proceedings of the 2013 International Conference on Mechatronics and Automatic Control Systems (ICMS2013) , Springer International Publishing, (2013) pp. 363-372.
DOI: 10.1007/978-3-319-01273-5

[11] D. Petcu, PVMaple: A Distributed Approach to Cooperative Work of Maple Processes, in J. Dongara et al (Eds) Recent Advances in Parallel Virtual Machine and Message Passing Interface: Seventh European PVM/MPI Users' Group Meeting, Balatonfüred, Hungary, September 10-13, 2000 Proceedings, Springer-Verlag Berlin Heidelberg, (2000), pp. 216–224.

[12] D. Petcu, Numerical Solution of ODEs with Distributed Maple", in L. Vulkov et al (Eds), Numerical Analysis and Its Applications: Second International Conference, NAA 2000 Rousse, Bulgaria, June 11-15, Revised Papers, (2000), pp. 666-674.

[13] R. Martinez, R. Pena: Building an Interface Between Eden and Maple: A way of Parallelizing Computer Algebra Algorithms, in P. Trinder et al (Eds) Implementation of Functional Languages 15th International Workshop IFL

2003 Edinburgh, UK, September 8-11, 2003. Revised Papers, Springer-Verlag Berlin Heidelberg, (2005), pp. 135-151.
DOI: 10.1007/978-3-540-27861-0_9

[14] W. Schreiner, C. Mittermaier, K. Bosa, Distributed Maple: parallel computer algebra in networked environments, in H Hong (editor) Journal of Symbolic Computation, 35 (3) (2003), pp. 305–347.
DOI: 10.1016/S0747-7171(02)00137-2

[15] D. Petcu, Numerical Solution of ODEs with Distributed Maple", in L. Vulkov et al (Eds), Numerical Analysis and Its Applications: Second International Conference, NAA 2000 Rousse, Bulgaria, June 11-15, Revised Papers, (2000), pp. 666-674.

[16] D. Petcu, M. Paprzycki, D. Dubu, Design and implementation of a grid extension for Maple, Scientific Programming, 13 (2) IOS Press, (2005) pp. 137–149.
DOI: 10.1155/2005/653638

[17] G. M. Díaz-Toca, A. L. Murica, Berkowitz Algorithm in parallel with the Maple Grid Computing Toolbox [cited 28.12.2017]
http://dis.um.es/~domingo/08/CD/27May/Posters/ALopez/poster.pdf
[accessed 28.12.2017]

[18] Gy. Molnárka, L. Gergó, F. Wettl, A. Horváth, G. Kallós, Maple V and its applications, Springer Hungarica, Budapest, (1996) in Hungarian

[19] R. Cypher, J. L.C. Sanz, The SIMD Model of Parallel Computation, Springer-Verlag New York, (1994), pp. 1-3.
DOI: 10.1007/978-1-4612-2612-3

[20] W.Auzinger, Demonstration of a parallel computation in Maple using the Grid package, TU Wien:, lecture notes, 2016, [cited 25.10.2016]
http://www.asc.tuwien.ac.at/compmath/2016/Grid-Demo.pdf

[21] L. Környei, G. Kallós, D. Fülep: Parallel Computations on the Blade Server at Széchenyi István University, Acta Technica Jaurinensis, 3 (1) (2010) pp. 111-126.

[22] G. Lencse, I. Derka: Testing the Speed-up of Parallel Discrete Event Simulation in Heterogeneous Execution Environments In: Veronique Limère , El-Houssaine Aghezzaf (Eds.) Proceedings of the ISC'2013, 11th Annual Industrial Simulation Conference, (2013) pp. 101-107.

[23] Hajdu, Gy. Molnárka: Numerical examination of a system model with a nonlinear component, in TEAM 2016: Proceedings of the 8th International Scientific and Expert Conference, AlumniPress, (2016), pp. 12-16.

[24] E.Miletics, Gy. Molnárka: Taylor series method with numerical derivatives for initial value problems, Journal of Computational Methods in Sciences and Engineering, 4 (1-2) (2004) pp. 105-114.

[25] G.A. Gravvanis, B.E. Moutafis, C.K. Filelis-Papadopoulos, H.G. Theodosiou: Parallel Semi-Aggregation Techniques for Solving Parabolic Partial Differential Equations, in P. Iványi, B.H.V. Topping and G. Várady, (Eds), Advances in Parallel, Distributed, Grid and Cloud Computing for Engineering, Saxe-Coburg Publications, Stirlingshire, UK, Chapter 8, (2017) pp 157-182.
DOI:10.4203/csets.40.8

[26] F.Hajdu, Cs. Hajdu: Parallelization of numerical creation of phase-plane diagram of a simple nonlinear system, (in Hungarian), in G. Keresztes (Ed) Proceeding of spring wind conference 2, Miskolc, (2017), pp.547-557.

[27] P. L. Simon, H. Farkas, M. Wittmann, Constructing global bifurcation diagrams by the parametric representation method, Journal of Computational and Applied Mathematics, 108 (1-2) (1999) pp.157-176.
DOI: 10.1016/S0377-0427(99)00108-9

[28] S. Lynch, Dynamical Systems with Applications using Maple, Birkhäuser Boston, (2010), pp. 143-165.
DOI: 10.1007/978-1-4899-2849-8

[29] F. Hajdu, Parallel numerical creation of 2-parametric bifurcation diagram of nonlinear oscillators, Acta Technica Jaurinensis, 11 (2) (2018) pp. 61-83.
DOI: 10.14513/actatechjaur.v11.n2.453

[30] S. A. Billings, O.M. Boaghe, The response spectrum map, a frequency domain equivalent to the bifurcation diagram, International Journal of

Bifurcation and Chaos, 11 (7) (2001) pp. 1961-1975.
DOI: 10.1142/S0218127401003164

Acta
Technica
Jaurinensis

Vol. 11, No. 3, pp. 150-164, 2018
DOI: 10.14513/actatechjaur.v11.n3.469
Available online at acta.sze.hu

Investigation of Long Cellulose Fibre Reinforced and Injection Moulded Poly(lactic acid) Biocomposites

S. Hajba[1], T. Tábi[1,2]

[1]Budapest University of Technology and Economics, Department of Polymer Engineering
Muegyetem rkp. 3., 1111 Budapest, Hungary
e-mail: hajba@pt.bme.hu

[2]MTA–BME Research Group for Composite Science and Technology
Muegyetem rkp. 3., 1111 Budapest, Hungary

Abstract: We investigated injection moulded composites of a polylactic acid matrix reinforced with cellulose fibers. We produced long fiber reinforced granules (preforms) with the use of two technologies: extrusion coating and film stacking. We examined the effect of fiber reinforcement and manufacturing technology on the properties of the composites. 30 wt% fiber reinforcement caused an increase in both strength and modulus compared to the reference PLA, and we also managed to improve creep resistance.

Keywords: poly(lactic acid), biopolymer, biocomposite, cellulose fiber, injection moulding

1. Introduction

Nowadays even though crude oil prices are going down, the amount of bioplastics sold keep on growing and a great deal of effort is spent on their development, therefore more and more research projects focus on a biopolymer. According to estimates, petroleum reserves are enough for another 40 years or so but as crude oil is running out; its price is going to go up, making petroleum-based plastics more expensive, too. Although only 5-6% of crude oil is used by the plastic industry each year, it is important to research for alternatives to replace petroleum-based polymers. Another serious problem is waste management, as conventional polymers take a very

long time to decompose or do not decompose at all, and therefore present an enormous load on the environment. The use of biopolymers [1] (biodegradable polymers produced from renewable resources) can solve this problem; at the end of their lifetime, they can be decomposed into humus, water and carbon dioxide in the proper environment. However, some biopolymers have properties inferior to those of conventional polymers or are more expensive than petroleum-based polymers, which limits their widespread use. A prominent representative of biopolymers is polylactic acid (PLA), which is most similar to polyethylene terephthalate (PET) and polystyrene (PS) in terms of its structure and properties. Its high strength (50-60 MPa) and rigidity (3-4 GPa) make it stand out from other biopolymers but still, it is most extensively used in the packaging industry [2][3][4][5][6][7]. Creating composites is one way of making PLA suitable for engineering applications. If cellulose-based fibers are used as reinforcement [8][9][10][11][12][13], the composite will completely retain the biodegradability of PLA.

With the use of natural fibers, strength, modulus and impact strength can be improved, and the composite will also be biodegradable. Many papers have focused on PLA composites with various cellulose-based fibers as reinforcement, such as flax, hemp, cotton, jute, kenaf, and other natural and artificial cellulose fibers. A critical point of PLA composites reinforced with cellulose-based fibers is fiber-matrix adhesion – its quality greatly affects the properties of the composite. It may happen that the strength of the composite is lower than that of the matrix even in the case of 47 vol% reinforcement [14]. Researchers have used numerous surface treatment agents to improve adhesion between cellulose-based fibers and PLA [14][15][16][17][18][19][20]. Sawpan et al [15] investigated the effect of surface treatment on interfacial shear strength (IFSS) in the case of hemp and PLA. They subjected the fibers to alkali (PLA/ALK), silane (PLA/SIL), acetyl (PLA/ACY), maleic anhydride (PLA/MA), and combined alkali-silane (PLA/ALKSIL) surface treatment. They explained the difference between the different kinds of surface treatments with the OH side groups of the treated fiber, with which they can connect to the carbonyl and carboxyl groups of the PLA. Treatment with acetyl and maleic anhydride did not result in much improvement – researchers explained this with the fact that in the two surface treatments, the OH groups of the fiber are replaced by CH3CO (acetate), and COOH (carboxyl) groups, as a result of which fewer OH groups can contribute to interfacial adhesion. Tokor et al [16] performed a similar IFSS test on bamboo fibers treated with an alkali and steaming, and Cho et al [17] as well, on jute and kenaf fibers treated with static and dynamic soaking. In both cases, the researchers showed that surface treatment improved adhesion, which was indicated by the increase in interfacial shear strength. Huda et al [14] investigated the effect of alkali and silane surface treatment on kenaf/PLA composites. As fiber content increased, flexural modulus increased as well, but strength decreased

initially, which the researchers attributed to the inferior adhesion between the fibers and the PLA. The alkali/silane combined surface treatment resulted in a considerable increase of modulus from 27 vol%, and all surface treatments led to better mechanical properties. However, even this increased strength is less than the strength of PLA, which can be attributed to the structural damage and strength decrease of the kenaf fibers as a result of surface treatment. Surface treatment on the other hand, considerably improved the notched Izod impact strength of the composites (alkali treatment improved it by 50%), and the heat deflection temperature also increased from 65 °C to 174 °C), which the researchers attributed to improved fiber-matrix adhesion. This, however, should be viewed critically because the PLA they used had a melting temperature range of 150-180 °C. Storage modulus increased more than 100% as a result of the combined surface treatment.

In the literature, the most commonly used method to produce biocomposites is film stacking [18][19][20][21][22]. Its advantage is that up to 70 wt% fiber content can be achieved, as opposed to the 30 wt% achievable by injection moulding, which allows considerable improvement in properties. Ochi's [19] 70 wt% kenaf-reinforced composites manufactured by film stacking had a tensile strength of 223 MPa and a flexural strength of 254 MPa; modulus values were around 22 GPa. in spite of the considerable improvement, he also mentions imperfect adhesion.

Injection moulding can produce products of far more complicated geometry than film stacking but maximum fiber content and fiber length are lower as during extrusion and injection moulding, fibers are broken. Bledzki et al [23][24] compared injection moulded polypropylene and polylactic acid based biocomposites with 30 wt% fiber content. They found that the best composite was cellulose fiber reinforced PLA both in terms of strength and impact strength. The researchers attributed this to the far more uniform quality of regenerated cellulose than that of plant fibers, and also mentioned that fiber matrix adhesion is critical, and that too high processing temperatures can cause the cellulose fibers to degrade. The achievable maximum tensile strength and modulus are lower than in the case of film-stacked composites; tensile strength was 92 MPa and modulus was 6.5 GPa. Many research projects [25][26][27][28] yielded similar results; lower fiber content than in the case of film stacking results in less improvement in strength and other properties.

Based on the literature, it can be concluded that in the case of these biocomposites, the most important task is to create proper adhesion. If adhesion is good, fiber reinforcement can considerable improve the strength, impact strength and heat deflection temperature of PLA. In some cases, however, the strength of the fiber-reinforced composite did not even reach that of pure PLA. Many surface treatment agents have been tried but alkali and silane treatment proved the best. A great

disadvantage of surface treatment agents is that they are poisonous and dangerous; therefore, their application is complicated and treatment takes a long time. In most cases, the composites were manufactured by film stacking, which greatly improved strength parameters due to high fiber content. Injection moulding was only used in a few cases, mostly due to the low achievable fiber content.

2. Materials and methods

Injection moulding grade PLA type 3052D from NatureWorks was used in our research with a D-Lactide content of around 4%. 3052D PLA has a density of 1.24 g/cm3, a T_g range of 55-60 °C, a melting temperature range of 145-160 °C and a melt flow index of 14 g/10 min (at 210 °C, with a 2.16 kg load). PLA was dried for 6 hours at 80°C before biocomposite production. We used Viscord Bohemia Super 2 type regenerated cellulose fibers from Glanzstoff Bohemia. Its linear density is 2440 dtex, the number of fibers in a roving is 1320.

The long fiber preforms necessary for the tests were prepared with two technologies (Fig. 1.). One was extrusion coating. We produced the long-fiber granules with a coating tool fitted to a Labtech LTE 26-44 twin-screw extruder, and fiber puller and pelletizer connected to it. We varied fiber content by modifying the rotational speed of the extruder, the fiber pulling speed, and the amount of fibers entered into the die. At an extruder screw rotational speed of 10 1/min and a pulling speed of 12 m/min, in the case of 2 cellulose rovings, fiber content was 15 wt%, while in the case of 4 cellulose rovings, it was 30 wt%. The other method of making long-fiber granules was film stacking, with which we produced thin sheets containing 30 wt% fibers. We then cut these sheets into 10 mm long pieces.

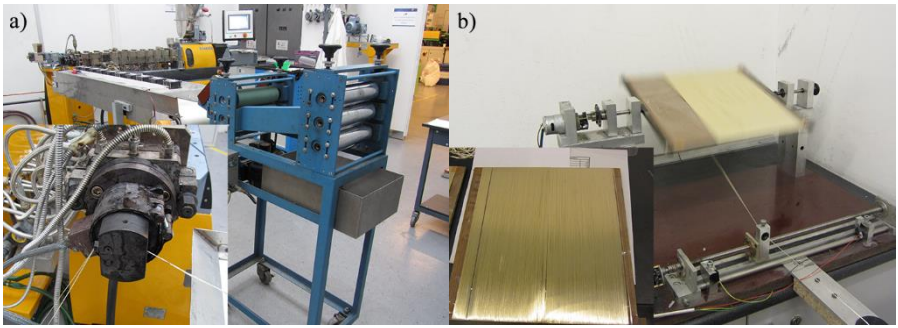

Figure 1. PLA/cellulose composite preform manufacturing: extrusion coating a) and winding plus film stacking b)

10 mm initial pellet length were used since it was possible to make this pellet size in both technologies. Additionally, higher than 10 mm and lower than 5 mm pellet

lengths were also investigated in a tests not presented in this paper, since both pellet length ranges were rejected. The usage of higher pellet length was rejected due to very high fibre distribution inhomogeneity, while the usage of lower pellet length was also rejected since the fibres pull-out from the pellets during cutting. Accordingly, in our paper, based on these previous tests, the effect of initial pellet length of 5, 7, and 10 mm was investigated. The specimens were produced by injection moulding from types of both long-fiber granules. An Arburg Allrounder 370S 700-290 injection moulding machine was used for this. Melt temperature was 170-230 °C, and mold temperature was 25 °C. Shot volume was 43 cm^3, switchover volume was 12 cm^3, screw rotational speed was 15 m/min, holding pressure and holding time were 600 bar and 20 s, and residual cooling time was 40 s. The designation of samples produced by coating and injection moulding was C+IM, while the designation of samples made by film stacking and injection moulding was HP+IM.

Differential Scanning Calorimetry measurements were performed on a TA Instruments Q2000 type calorimeter (NewCastle, USA). 3–6 mg samples were taken from the middle of the cross-section of the injection moulded specimens. Firstly, we took the samples from unannealed injection moulded specimens and performed isothermal measurements to determine necessary annealing times. Secondly, after annealing the injection moulded specimens for various times or at various temperatures, we examined the samples in non-isothermal mode (heat/cool/heat) from 0 to 200 °C at a heating/cooling rate of 5 °C/min to determine the glass transition temperature (T_g), cold crystallization temperature (T_{cc}), enthalpy of cold-crystallization (ΔHcc), melting temperature (T_m), and the enthalpy of fusion (ΔHm). Crystallinity was calculated from the first heating scan of the injection moulded specimens with Eq. (1):

$$X_c = \frac{\Delta H_m - \Delta H_{cc}}{\Delta H_f \cdot (1-a)} \cdot 100\%, \qquad (1)$$

where X_c (%) is the calculated crystallinity, ΔH_m (J/g) and ΔH_{cc} (J/g) are the enthalpy of fusion and the enthalpy of cold crystallization, respectively, a [-] is fiber content, and ΔH_f (J/g) is the enthalpy of fusion for 100% crystalline PLA (93.1 J/g) [3].

Heat Deflection Temperature measurements were performed on a Ceast HV3 type HDT (Torino, Italy) measuring equipment, according to the ISO 75:2013 standard. HDT B type measurements were carried out in flatwise mode with a loading stress of 0.45 MPa, heating rate of 2 °C/min (120 °C/hour) and with a span length of 64 mm.

The mechanical properties of the annealed and unannealed PLA specimens were analyzed with tensile, flexural and Charpy tests, based on MSZ EN ISO 527:2012,

MSZ EN ISO 178:2011 and MSZ EN ISO 179:2010 respectively. The tensile and the flexural tests were performed on a Zwick Z020 universal testing machine (Ulm, Germany), equipped with a Zwick BZ 020/TN2S force measuring cell with a force limit of 20 kN, with a crosshead speed of 5 mm/min. The Charpy impact tests were performed on unnotched samples with a Ceast Resil Impactor (Torino, Italy) impact testing machine equipped with a 2 J impact energy hammer and a DAS8000 data collector unit. All of the tests were performed at room temperature and at a relative humidity of 50 ± 10%.

Scanning electron microscopy (SEM) was performed with a Jeol JSM 6380LA type electron microscope. The fracture surfaces of the tensile specimens were used for the observations. An Au/Pd alloy was sputtered onto the surface prior to observation to avoid electrostatic charging.

3. Results and discussion

After coating it can be seen that fiber reinforcement is in the middle, and it is surrounded by the PLA matrix. The image of higher magnification clearly shows that there is little PLA between the introduced fiber bundles. The dispersion of fibers during injection moulding may be made more difficult by the fact that the fiber bundle remained as one whole after coating. (Fig. 2.).

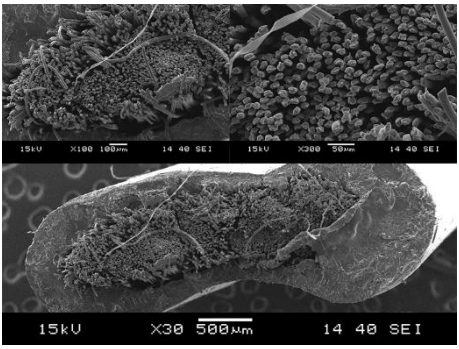

Figure 2. The structure of the composite preform made with extrusion coating

In the case of the preform produced by film stacking (Fig. 3.), the fiber bundles do not form a whole unit so much and there is matrix material between the fibers. This way during subsequent injection moulding, the fibers can be dispersed better, which can result in better properties of the composite.

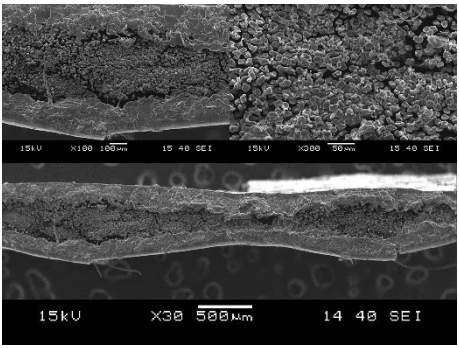

Figure 3. The structure of the composite preform made with film stacking

First, we performed tensile, flexural and Charpy impact tests on the long-fiber injection moulded PLA/cellulose composites. The average fiber content of the composites was 15 and 30 wt%. We managed to achieve improvement in strength and impact strength with the use of cellulose fibers even at low fiber content (~15 wt%). Cellulose fibers did not improve tensile strength and modulus much, but they increased flexural strength from 97.8 MPa to 133.3 MPa, and modulus from 3.4 GPa to 5.3 GPa (Fig. 4.). At higher fiber content, tensile elasticity modulus decreased due to the inferior dispersion of fibers (Fig. 4).

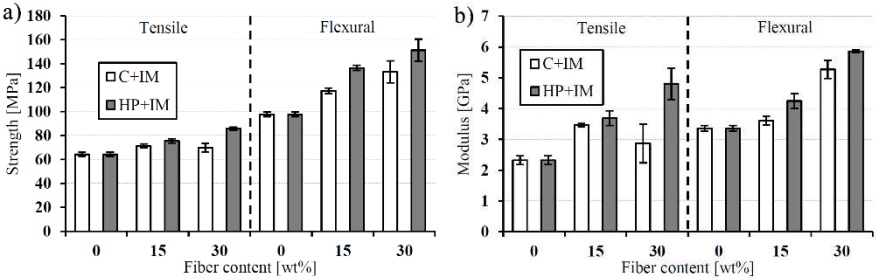

Figure 4. PLA/cellulose strength a) and modulus b)

Cellulose fibers improved both Charpy impact strength and thermal dimensional stability. In the case of both properties, PLA and the composite had the roughly same values up 15 wt% fiber content, while both the toughness and heat deflection temperature of the composite containing 30 wt% fibers increased. Charpy impact strength doubled and the heat deflection temperature increased by 25 °C (Fig. 5.).

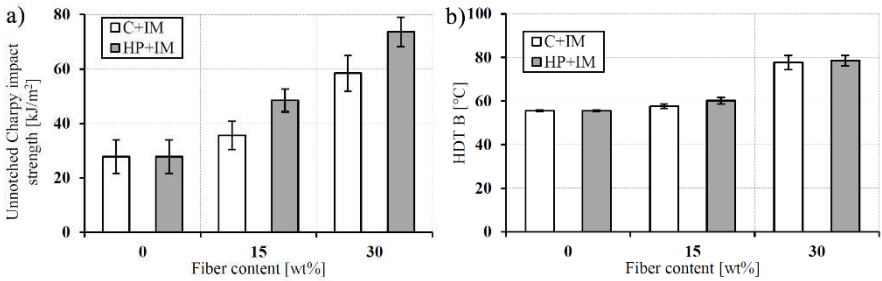

Figure 5. PLA/cellulose composites Charpy impact strength a) and heat deflection temperature (HDT) b)

Cellulose fibers can improve resistance to creep compared to pure PLA (Fig. 6.). At a load of 30 wt%, the lifetime of composites injection moulded from film-stacked preforms is considerably longer, thanks to the better dispersed fibers in the composite. Obviously, the neglections applied by the approximation method, such as ambient temperature and its deviations, UV radiation and its effects, degradation and mechanical impacts have to be taken into account.

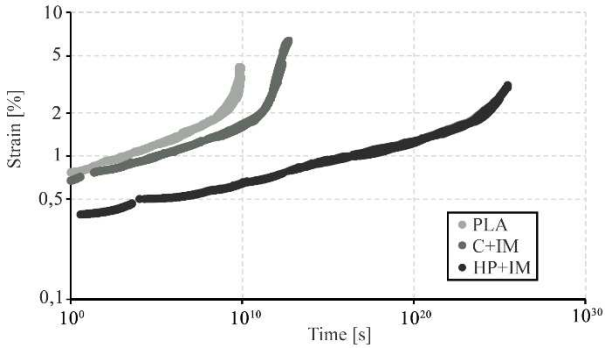

Figure 6. The master creep curves of PLA and long-fiber reinforce, injection moulded composite for a load level of 30%

In the case of composites, we examined the effect of injection moulding parameters (melt temperature, injection speed, back pressure, screw rotational speed, initial granule length) on the properties of the composites. The results indicate that an increase in melt temperature (Fig. 7.), and injection speed (Fig. 8.), and a decrease in initial granule length (Fig. 9.) resulted in increased tensile strength and tensile elasticity modulus but did not affect Charpy impact strength. When melt temperature

was increased from 170 °C to 230 °C, both tensile and flexural strength increased by nearly 30 MPa, but modulus did not change much.

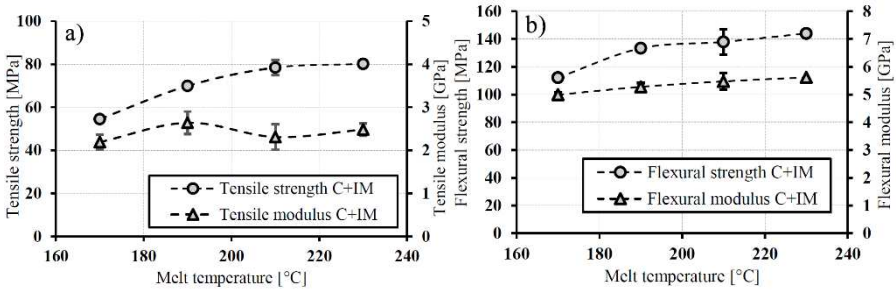

Figure 7. The effect of melt temperature on tensile a) and flexural b) strength and modulus

Reducing injection speed has a beneficial effect on the strength of the composite; probably because fiber breaking is reduced. Reducing injection speed to 10 cm^3/s led to an increase in tensile strength by nearly 15 MPa.

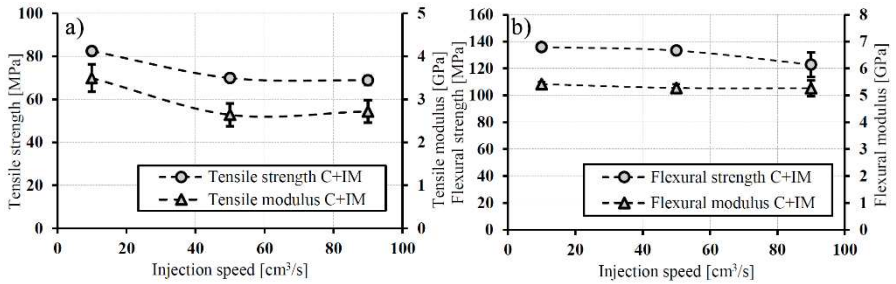

Figure 8. The effect of injection speed on tensile a) and flexural b) strength and modulus

The initial length of the long fiber granules affected the properties of the composite. Contrary to our expectations, the shorter pellet length was more effective in reinforcing capability due to the fact that shorter fibres could be more uniformly distributed in the specimens during injection moulding, while the long pellets caused inhomogeneity and increased stress concentration. The tensile and flexural strength of composites injection moulded from the shorter, 5 mm granules were slightly higher (by about 10 MPa) than in the case of the 10 mm granules. This is due to the fact that shorter fibers stick together less and are easier to disperse than longer fibers, which are more likely to form bundles, which also act as defect (Fig. 10.). A table has been constructed to present the results of Figure 7, 8 and 9 numerically.

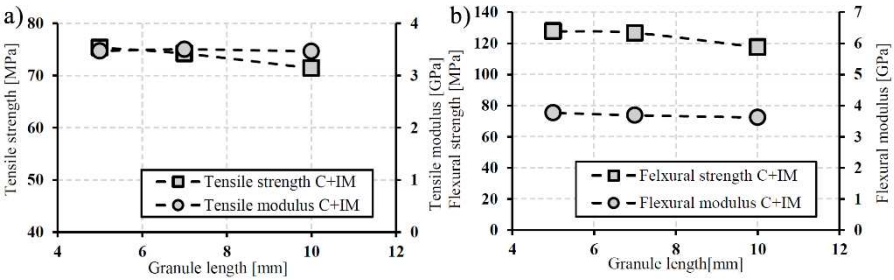

Figure 9. The effect of the initial length of the granules on tensile a) and flexural b) strength and modulus

Table 1. Mechanical properties of the injection molded composites

Properties	Melt temperature [°C]				Injection speed [cm^3/s]			Granule length [mm]		
	170	190	210	230	10	50	90	5	7	10
Tensile strength [MPa]	54,5 ±9,5	69,9 ±1,8	78,4 ±3,6	80,1 ±2,6	82,4 ±1,6	69,9 ±1,8	68,8 ±2,1	75,4 ±1,1	74,2 ±0,8	71,4 ±1,8
Tensile modulus [GPa]	2,2 ±0,2	2,6 ±0,3	2,3 ±0,3	2,5 ±0,1	3,5 ±0,3	2,6 ±0,3	2,7 ±0,3	3,5 ±0,1	3,5 ±0,1	3,5 ±0,1
Flexural strength [MPa]	112,2 ±7,2	133,3 ±4,6	137,9 ±4,5	144,0 ±5,2	135,9 ±2,2	133,3 ±4,6	122,9 ±2,7	127,8 ±1,5	126,7 ±2,0	117,4 ±2,3
Flexural modulus [GPa]	5,0 ±0,2	5,3 ±0,2	5,5 ±0,2	5,6 ±0,2	5,4 ±0,2	5,3 ±0,2	5,3 ±0,1	3,8 ±0,2	3,7 ±0,2	3,61 ±0,1

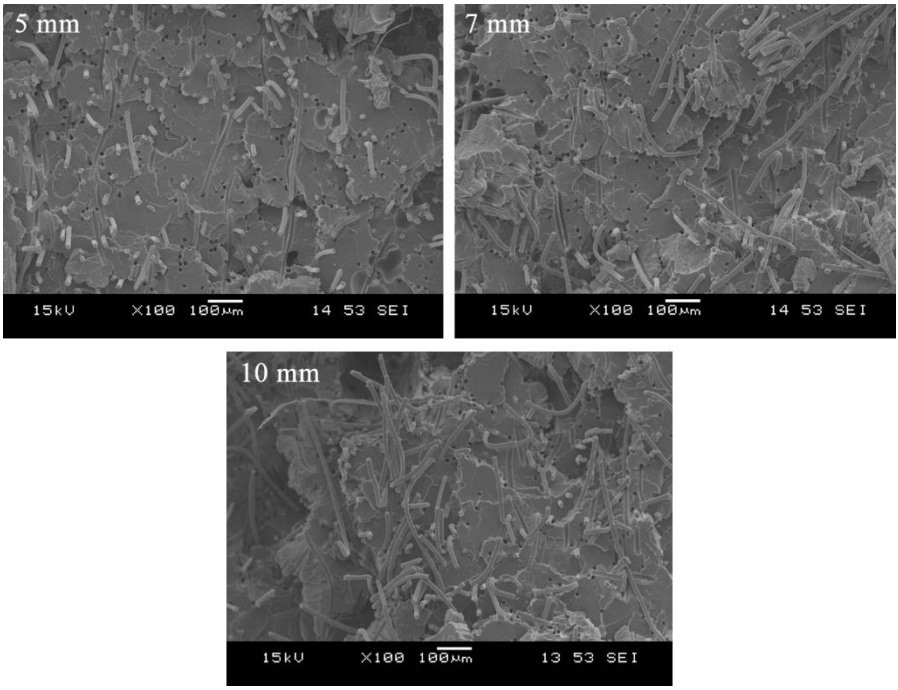

Figure 10. The fracture surfaces of injection moulded composites moulded from granules of different lengths (5 7, 10 mm)

Summary

In our work we produced long fiber reinforced granules with two different technologies for injection moulding. The maximum fibre content was 30 wt%. Due to the long fibre reinforcement both the strength and the modulus were increased by 40% and 50% respectively. Also the creep resistance was better of the composites compared to the neat PLA. Heat deflection temperature was also increased by 23 °C up to 78 °C.

Acknowledgement

The This research was supported by The National Research, Development and Innovation Office (NVKP_16-1-2016-0012). The authors thank Arburg Hungária Kft. for the Arburg Allrounder 370S 700-290 injection moulding machine, Lenzkes GmbH for the clamping tool system as well as Piovan Hungary Kft. and Tool-Temp Hungária Kft. for their support.

NATIONAL RESEARCH, DEVELOPMENT AND INNOVATION OFFICE
HUNGARY
PROJECT FINANCED FROM THE NRDI FUND
MOMENTUM OF INNOVATION

References

[1] G. Dogossy, T. Czigany, Thermoplastic starch composites reinforced by agricultural by-products: properties, biodegradability, and application, Journal of Reinforced Plastics and Composites 30 (21) (2011) pp. 1819-1825. DOI: 10.1177/0731684411429728

[2] D. Garlotta, A Literature review of poly(lactic acid), Journal of Polymers and the Environment, 9 (2) (2001) pp. 63-84. DOI: 10.1023/A:10202008

[3] L-T. Lim, R. Auras, M. Rubino, Processing technologies for poly(lactic acid), Progress in Polymer Science 33 (8) (2008) pp. 820-852. DOI: 10.1016/j.progpolymsci.2008.05.004

[4] R. M. Rasal, A. V. Janorkar, D. E. Hirt, Poly(lactic acid) modifications, Progress in Polymer Science 35 (3) (2010) pp. 338-356. DOI: 10.1016/j.progpolymsci.2009.12.003

[5] F. Carrasco, P. Pages, J. Gámez-Pérez, O. O Santana, M. L. Maspoch, Processing of poly(lactic acid): Characterization of chemical structure, thermal stability and mechanical properties, Polymer Degradation and Stability 96 (2) (2010) pp. 116-125. DOI: 10.1016/j.polymdegradstab.2009.11.045

[6] G. Dogossy, Polymer foams, in: Zsoldos I (Ed.), Chapters on the latest automotive research areas of non-metallic materials, Széchenyi István University, Győr, 2015, pp. 212-245, in Hungarian.

[7] G. Dogossy, F. Ronkay, Foaming of recycled PET, in: Csibi-Venczel J (Ed.), OGÉT 2013: 21st International Conference on Mechanical Engineering,

Erdélyi Magyar Műszaki Tudományos Társaság, Arad, pp. 97-100, 2013, in Hungarian.

[8] A. Bismarck, S. Mishra, T. Lampke, Plant Fibers as Reinforcement for green composites in: A. K. Mohanty, M. Misra, L. T. Drzal (eds): Natural fibers, biopolymers, and biocomposites, 1st edition, Taylor and Francis Group, Boca Raton, 2005, pp. 39-97.

[9] M. Ho, H. Wang, J. H. Lee, C. Ho, K. Lau, J. Leng, D. Hui, Critical factors on manufacturing process of natural fiber composites, Composites: Part B, 43 (8) (2012) pp. 3549-3562.
DOI: 10.1016/j.compositesb.2011.10.001

[10] S. Hajba,T. Czigany, T. Tábi, Development of cellulose-reinforced Poly(Lactic Acid) (PLA) for engineering applications, Materials Science Forum 812 (1) (2015) pp. 59-64.
DOI: 10.4028/www.scientific.net/MSF.812.59

[11] T. Mukherjee, N. Kao, PLA based biopolymer reinforced with natural fibre: A review, Journal of Polymer and Environment 19 (3) (2011) pp. 714-725.
DOI: 10.1007/s10924-011-0320-6

[12] L. Shen, E. Worrell, M. K. Patel, Environmental impact assessment of man-made cellulose fibres, Resources, Conservation and Recycling, 55 (2) (2010) pp 260-274.
DOI: 10.1016/j.resconrec.2010.10.001

[13] P. White, M. Hayhurst, J. Taylor, A. Slater, Lyocell fibres, in: R. S. Blackburn (ed.): Biodegradable and sustainable fibres, 1st edition, Woodhead Publishing Limited, Cambridge, 2005, pp. 157-188.

[14] M. S. Huda, L. T. Drazal, A. K. Mohanty, M. Misra, Effect of fiber surface-treatments on the properties of laminated biocomposites from poly(lactic acid) (PLA) and kenaf fibers, Composites Science and Technology 68 (2) (2008) pp. 424-432.
DOI: 10.1016/j.compscitech.2007.06.022

[15] M. A. Sawpan, K. L. Pickering, A. Fernyhough, Effect of fibre treatments on interfacial shear strength of hemp fibre reinforced polylactide and unsaturated polyester composites, Composites: Part A 42 () (2011) pp. 1189-1196.
DOI: 10.1016/j.compositesa.2011.05.003

[16] R. Tokoro, D. M. Vu, K Okubo, T. Tanaka, T. Fujii, T. Fujiura, How to improve mechanical properties of polylactic acid with bamboo fibres, Journal of Materials Science 43 (2) (2008) pp. 775-787.
DOI: 10.1007/s10853-007-1994-y

[17] D. Cho, J. M. Seo, H. S. Lee, C. W. Cho, S. O. Han, W. H. Park, Property improvement of natural fibre reinforced green composites by water treatment, Advanced Composite Materials 16 (4) (2007) pp. 299-314.
DOI: 10.1163/156855107782325249

[18] T. Nishino, K. Hirao, M. Kotera, K. Nakamae, H. Inagaki, Kenaf reinforced biodegradable composite, Composites Science and Technology 63 (9) (2003) pp. 1281-1286.
DOI: 10.1016/S0266-3538(03)00099-X

[19] S. Ochi, Mechanical properties of kenaf fibres and kenaf/PLA composites, Mechanics of Materials 40 (4-5) (2008) pp. 446-452.
DOI: 10.1016/j.mechmat.2007.10.006

[20] X. Li, G. L. Tabil, S. Panigrahi, Chemical treatments of natural fiber for use in natural fiber reinforced composites: A review, Journal of Polymer and Environment 15 (1) (2007) pp. 25-33.
DOI: 10.1007/s10924-006-0042-3

[21] N. Graupner, A. S. Hermann, J. Müssig, Natural and man-made cellulose fibre-reinforced poly(lactic acid) (PLA) composites: An overview about mechanical characteristics and application areas, Composites: Part A 40 (6-7) (2009) pp. 810-820.
DOI: 10.1016/j.compositesa.2009.04.003

[22] K. Oksman, M. Skrifvars, J.-F Selin, Natural fibres as reinforcement in polylactic acid (PLA) composites, Composites Science and Technology 63 (9) (2003) pp. 1317-1324.
DOI: 10.1016/S0266-3538(03)00103-9

[23] A. K. Bledzki, A. Jaszkiewicz, Mechanical performance of biocomposites based on PLA and PHBV reinforced with natural fibres – A comparative study to PP, Composites Science and Technology 70 (12) (2010) pp. 1687-1696.
DOI: 10.1016/j.compscitech.2010.06.005

[24] A. K. Bledzki, A. Jaszkiewicz, D. Scherzer, Mechanical properties of PLA composites with man-made cellulose and abaca fibres, Composites: Part A 40 (4) (2009) pp. 404-412.
DOI: 10.1016/j.compositesa.2009.01.002

[25] B. Asaithambi, G. Ganesan, S. Ananda Kumar, Bio-composites: Development and Mechanical Characterization of Banana/Sisal Fibre Reinforced Poly Lactic Acid (PLA) Hybrid Composites, Fibers and Polymers 15 (4) (2014) pp. 847-854.
DOI: 10.1007/s12221-014-0847-y

[26] A. A. Yussuf, I. Massoumi, A. Hassan, Comparison of polylactic acid/kenaf and polylactic acid/rise husk composites: The influence of the natural fibers on the mechanical, thermal and biodegradability properties, Journal of Polymers and Environment 18 (3) (2010) pp. 422-429.
DOI: 10.1007/s10924-010-0185-0

[27] N. C. Loureiro, J. L. Esteves, J. C. Viana, S. Ghosh, Development of polyhydroxyalkanoates/poly(lactic acid) composites reinforced with cellulosic fibers, Composites: Part B 60 (1) (2014) pp. 603-611.
DOI: 10.1016/j.compositesb.2014.01.001

[28] B. Bax, J. Müssig, Impact and tensile properties of PLA/Cordenka and PLA/Flax composites, Composites Science and Technology 68 (7-8) (2008) pp. 1601-1607.
DOI: 10.1016/j.compscitech.2008.01.004